Nuclear Equipotential Surfaces in the Heavy Elements*

Richard R. Chasman
Chemistry Division, Argonne National Laboratory, Argonne, Illinois 60439
(Received 20 October 1969)

The shifts of single-particle energy levels caused by distortions of nuclear equipotential surfaces is examined. Application of this approach is made to neutron single-particle states in the heavy-element region. Typical single-particle energy shifts are displayed in figures.

The equipotential shapes studied in this paper are axially symmetric and were obtained by the replacement

$$\omega_0^2 r^2 \rightarrow \omega_\rho^2 \rho^2 + \omega_z^2 z^2 + \omega_0^2 (\rho^2 + z^2) G(z^2)$$

with $G(z^2)$ of the form

$$G(z^2) = e^{-Az^2} \sum_n B_n (z^{2t})^n .$$

A Woods-Saxon well was used for the central field, and eigenstates of the cylindrical harmonic oscillator ($|n_\perp, \lambda, n_z\rangle$) were used as a basis set in these calculations. ^{235}U is analyzed in detail.

I. INTRODUCTION

With the development of one-particle transfer reactions as a spectroscopic tool, many rotational bands are being observed and identified in the heavy-element region. If we assume that the positions of the observed bands are determined by a single-particle Hamiltonian and residual pairing forces, it is possible to extract single-particle level orderings and energy spacings from these data. This affords us an opportunity to test and refine single-particle potential models in considerably more detail than has been the case heretofore. In this paper we discuss the following questions: (1) to what extent can single-particle level orderings and energy spacings be shifted by varying the shape of nuclear equipotential surfaces, and (2) how useful is this approach for improving the agreement between the predictions of single-particle models and experimental observations. We study axially symmetric equipotential surfaces, which deviate from purely ellipsoidal shapes. Our answer to the second question is quite provisional; we analyze only ^{235}U in detail in this paper. As analyses of experimental data are completed for other heavy nuclei, we hope to apply the same approach to them. The fundamental question to be raised concerning this approach is: as we analyze neighboring nuclei, how are the shifts in equipotential surface shape correlated with the last occupied nucleon orbital. Discussion of this question must also be deferred until more nuclei are analyzed.

The first equipotential surface, other than the spherical, to be studied was the ellipsoidal. This has been done for both a modified oscillator[1] and a Woods-Saxon[2] single-particle potential. More recently, equipotential surface deformations of the $P_4(\cos\theta)$ type[3] have been studied. In our calculations, we have used a Woods-Saxon well as the single-particle potential. As suggested by the work of the Dubna group,[4] we have used harmonic-oscillator eigenfunctions as our basis set. Our calculation differs from theirs in that we have used cylindrical oscillator[5] eigenfunctions ($|n_\perp, \lambda, n_z\rangle$) as our basis set rather than the spherical oscillator eigenfunctions. Also, we use a larger number (14) of oscillator shells in our calculations. The main motivation for using the cylindrical oscillator set is our expectation that equipotential surfaces of nuclei in the heavy-element region should exhibit small deviations from ellipsoidal shapes. This choice of basis set is also quite convenient for making a rather detailed examination of the effects of the deviations from ellipsoidal shape on single-particle energy level spacings. A secondary advantage of using the cylindrical basis set is the relative simplicity of the transformation[6] from single-particle coordinates to coordinates of relative motion and c.m. for this basis set. This feature is useful in residual-interaction calculations.

In Sec. II, we discuss the details of our calculation and in Sec. III, we display some results of the calculations. The major result is contained in Fig. 1. In Appendix A, we list some relations needed for the evaluation of matrix elements.

II. SINGLE-PARTICLE MODEL

The starting point for our calculation is the Woods-Saxon single-particle Hamiltonian[2]

$$H = \frac{P^2}{2m} - V_0 \left[\frac{1}{1 + e^{\alpha[(r/R_0)-1]}} \right] - K \vec{l} \cdot \vec{s} \left[\frac{1}{r} \frac{d}{dr} \left(\frac{1}{1 + e^{\alpha[(r/R_0)-1]}} \right) \right], \quad (1)$$

and the parameters of this model are V_0, α, r_0, and K; where r_0 is defined through the relation

$$R_0 = r_0 A^{1/3}. \tag{2}$$

We have used values of V_0, α, and r_0 in rough agreement with those of Ross, Mark, and Lawson.[7] In our calculations, we have used a value of 1.35×10^{-13} cm for r_0. This value seems somewhat large, but we find that it gives slightly better agreement with observed single-particle energy level spacings in ^{235}U than does a value of either 1.3 or 1.4×10^{-13} cm. The value of K is fixed in our calculation by experimental data on single-particle states which originate as $j_{15/2}$ in the spherical limit. It should be noted that when we deform the equipotential surfaces, $\vec{l}\cdot\vec{s}$ does not commute with $(1/r)dV/dr$. For these cases, we make the replacement in the Hamiltonian

$$\vec{l}\cdot\vec{s}\,\frac{1}{r}\frac{dV}{dr} \rightarrow \frac{1}{2}\left(\vec{l}\cdot\vec{s}\,\frac{1}{r}\frac{dV}{dr} + \frac{1}{r}\frac{dV}{dr}\vec{l}\cdot\vec{s}\right). \tag{1'}$$

In order to utilize the cylindrical oscillator basis set in our calculations, it is extremely useful to rewrite the Woods-Saxon potential shape in the following way

$$\frac{1}{1+e^{\alpha[(r/R_0)-1]}} = \sum_l B_l e^{-C_l (r/R_0)^2}, \tag{3}$$

where the coefficients B_l and C_l are functions of α. We have found, through trial and error methods, that a 12-term expansion is sufficient to give a good fit to the Woods-Saxon shape for values of α appropriate to the heavy-element region. The difference between the right- and left-hand sides of Eq. (3) can be kept to less than 4×10^{-3} (i.e., ~150 keV) for all values of (r/R_0). We have also carried out a few calculations using a 16-term expansion, in which case the deviations are less than 1×10^{-3}, and our results appear quite insensitive to this refinement. By going through the intermediate step of Eq. (3) in our calculation, we have a program which can be readily used for any single-particle potential that can be expanded as a sum of terms $e^{-C_l r^2}$. Of course, the calculations are faster when the number of terms is few. After making the usual substitutions

$$\begin{aligned} p^2 &\rightarrow p'^2 \hbar\omega m, \\ r^2 &\rightarrow r'^2 \hbar/\omega m, \end{aligned} \tag{4}$$

the Hamiltonian of Eq. (1) has the form

$$H = \hbar\omega\left(\frac{p'^2}{2} - \frac{V_0}{\hbar\omega}\sum_l B_l e^{-C_l' r'^2} - \frac{K'}{\hbar\omega}\vec{l}\cdot\vec{s}\sum_l B_l C_l e^{-C_l' r'^2}\right), \tag{5}$$

where we have absorbed several quantities into C_l' and K', i.e.,

$$C_l' = C_l \hbar/\omega m R_0^2 \quad \text{and} \quad K' = -2K/R_0^2, \tag{6}$$

and $\hbar\omega$ is a characteristic harmonic-oscillator energy and determines the basis function set. Since we are using a large basis set, the eigenvalues we obtain are relatively insensitive to the choice of $\hbar\omega$. We have been using a value of $\hbar\omega = 6$ MeV which is optimum in the sense that intershell mixing of our eigenfunctions is roughly minimized for this choice; the eigenfunctions are typically 97% pure in terms of oscillator shell number.

At this point we consider the problem of equipotential surfaces. In order to get ellipsoidal equipotential surfaces, one makes the replacement

$$r^2 \rightarrow \rho^2 e^{2\epsilon/3} + z^2 e^{-4\epsilon/3} \tag{7}$$

with the parameter ϵ determining the shape of the ellipsoid. By defining ellipsoidal shapes in this way, volume conservation conditions are taken into account automatically. For the more general deformations in which we are interested, volume conservation considerations are not taken into account automatically; they appear to be of small importance, however, and we could correct for them approximately by conserving equipotential volume at a radius R_0 corresponding to the nuclear surface.

We find that we can represent many equipotential surface shapes rather conveniently by replacements of the form

$$r^2 \rightarrow \rho^2 e^{2\epsilon/3} + z^2 e^{-4\epsilon/3} + (\rho^2 + z^2) G(z^2/R_0^2), \tag{8}$$

with a function $G(z^2/R_0^2)$ of the form

$$G\left(\frac{z^2}{R_0^2}\right) = e^{-\gamma z^2} \sum_n A_n (z^{2t})^n, \tag{9}$$

where R_0^2 to various powers is absorbed into the constants γ and A_n. The quantities t and n are restricted to integral values in order to avoid mixing of states of opposite parity, and γ is an arbitrary parameter. As our program is now set up, the summation in Eq. (9) may contain up to six terms; this allows considerable flexibility in the choice of equipotential surface shapes. As a first step in seeing the possibilities of this approach, we might consider functions $G(z^2)$ consisting of a single term. By suitably choosing γ and t, it is possible to move the maximum of this function freely and to examine the effects on single-particle levels of distorting the equipotential surfaces at any point z_0. In Sec. III, we display the results of such calculations. In Fig. 5, we have plotted an equipotential surface shape which gives a set of single-particle levels in fairly good agreement

with those observed in ^{235}U; this gives some idea of the scale of the effects we are discussing here. Clearly, we are dealing with small deviations from ellipsoidal shapes.

Before carrying out the calculation, we transform to the stretched coordinate system via the substitutions

$$\rho^2 \to e^{-\epsilon/3}\rho'^2, \quad p_\rho{}^2 \to e^{\epsilon/3}p_\rho'^2,$$
$$z^2 \to e^{2\epsilon/3}z'^2, \quad p_z{}^2 \to e^{-2\epsilon/3}p_z'^2; \tag{10}$$

and when we include this substitution our Hamiltonian has the form

$$H=\hbar\omega\left\{(\tfrac{1}{2}p_\rho{}^2e^{\epsilon/3}+p_z{}^2e^{-2\epsilon/3}) - \frac{1}{\hbar\omega}\sum_l B_l(V_0+K'\vec{l}\cdot\vec{s}C_l)\right.$$
$$\left.\times\exp[-C_l'(\rho^2e^{\epsilon/3}+z^2e^{-2\epsilon/3})+(\rho^2+z^2)G(z^2)]\right\}; \tag{11}$$

where we have now dropped the primes from our variables z^2 and ρ^2, and we ignore the factors $e^{\epsilon/3}$ (and $e^{-2\epsilon/3}$) in the term $(\rho^2+z^2)G(z^2)$ as such factors amount only to a shift in the maximum of $G(z^2)$. The matrix elements of $\vec{l}\cdot\vec{s}$ are also affected by this transformation, and this is taken into account in the formulas of Appendix A.

We should point out that there is no necessity to make the transformation of Eq. (10); in fact, we have carried out a few calculations in the unstretched coordinate system. As we are using a large basis set, the eigenvalues we obtain are essentially the same in both coordinate systems. A difference between the two coordinate systems does show up when we examine the wave functions. In the stretched coordinate system, the wave functions are typically 97% pure in terms of shell number; when we use the unstretched coordinate system, the wave functions are ~92% pure in this respect.

In order to evaluate the matrix elements which arise in our calculation, we first make a power series expansion of the factor $\exp[-C_l'(\rho^2+z^2)G(z^2)]$. We have found that an expansion to fourth order is sufficient for the cases we have studied so far, and we have been carrying this expansion to fifth order in our program. After this expansion is carried out, the calculational problem is reduced to the evaluation of matrix elements of the form

$$\langle n_\perp,\lambda,n_z|(\rho^2)^{n_1}(z^2)^{n_2}e^{-a\rho^2}e^{-bz^2}|n_\perp',\lambda',n_z'\rangle,$$

which can be immediately factored to give products of the form

$$\langle n_\perp,\lambda|(\rho^2)^{n_1}e^{-a\rho^2}|n_\perp',\lambda'\rangle\langle n_z|(z^2)^{n_2}e^{-bz^2}|n_z'\rangle,$$

both terms of which may be evaluated analytically. To carry out the analytic integrations, we use the explicit forms of the basis functions $|n_\perp,\lambda\rangle$ and $|n_z\rangle$ which are given in Appendix A.

The programming involved in the diagonalization of the Hamiltonian is relatively straightforward and consists mostly of careful indexing. The main concern is to compute the matrix elements $\langle n_z|(z^2)^ne^{-bz^2}|n_z'\rangle$ as efficiently as possible, as there are so many matrix elements of this type which must be evaluated. All calculations have been done on a CDC-3600 computer, and the actual matrix diagonalizations were carried out using the subroutine AN F-202. Using a 14-shell basis set and a 12-term expansion for the Woods-Saxon shape, it takes ~100 sec to carry out the calculation for $G(z^2)=0$. When $G(z^2)$ consists of one term, the calculation takes roughly 140 sec and a slightly smaller increment of time (~22 sec) occurs for each additional term in $G(z^2)$. The estimates quoted above apply when we compute only eigenvalues; if we want eigenfunctions as well, another ~35 sec should be added to each estimate given above. The calculation is not extremely fast, but the length of time involved seems far from prohibitive in view of the results to be obtained from such calculations.

III. RESULTS

The major result of this paper is contained in Fig. 1. In this figure, we have plotted the energies of neutron single-particle states as a function of the value of z^2 for which $G(z^2)$ is at its maximum; we refer to this value of z^2 simply as $z^2{}_{\max}$. For the construction of this figure, we have taken a set of functions $G(z^2)$ with maxima spaced at intervals of 1 in z^2; all the functions are of the same sign (negative); and the coefficients of each function are chosen such that

$$\frac{1}{\sqrt{\pi}}\int_0^\infty G(z^2)dz \simeq -0.02\,. \tag{12}$$

No great significance should be attached to the value 0.02. The magnitude 0.02 was chosen as this seems to give shifts of roughly the right size to explain the changes in energy of experimentally observed levels from nucleus to nucleus. The magnitudes of single-particle energy level shifts can be changed by changing the magnitude of this coefficient. On the right-hand side of Fig. 1, we have included the single-particle energies obtained in the ellipsoidal limit [i.e., $G(z^2)=0.0$]. A rough rule of thumb is that changes in the magnitude of $G(z^2)$ will shift each level by an amount proportionate to the amount of its deviation from the ellipsoidal limit. Another rough rule is that changing the sign of $G(z^2)$ reflects a single-particle energy level about its value in the ellipsoidal limit. In Fig. 2, we have carried out this reflection to get a picture of how the single-particle levels shift

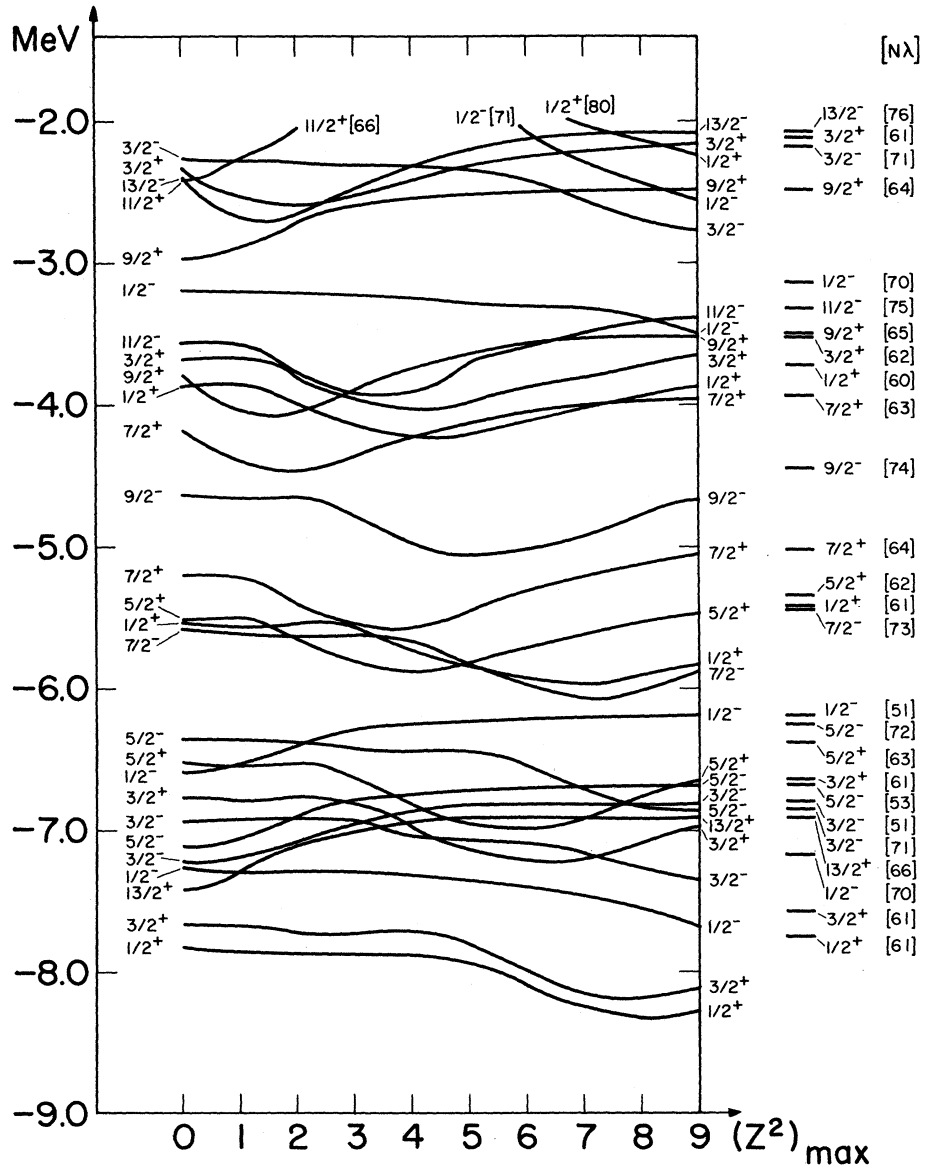

FIG. 1. Shifts of single-particle energies due to distortion of equipotential surfaces. The parameters used for this calculation are: $\epsilon = 0.23$, $V_0 = 39.2$ MeV, $r_0 = 1.35 \times 10^{-13}$ cm, $\alpha = 11.7$, $K' = 0.130$ MeV, and $\int_0^\infty G(z^2)dz \simeq -0.02$.

from positive $G(z^2)$; no additional calculations were done to construct Fig. 2.

A priori, we expect to see that single-particle states with about the same distribution of values of n_z will shift in approximately the same way as we vary $z^2{}_{\max}$; this is what we do see.

We have not made any detailed examinations of our wave functions as yet, but we have looked at their distributions in terms of N, the oscillator shell number, and λ, the projection of angular momentum on the z axis. The value of λ given as a label for each single-particle state corresponds to the dominant value in the wave function. The only real surprise in the level ordering of Fig. 1 is that the second state labeled $\frac{1}{2}^-[70]$ occurs at an energy lower than the first state $\frac{1}{2}^-[71]$; aside from this the single-particle levels are where we expect[3] them. If we know the distribution in λ of our wave functions, we also know $\langle S_z \rangle$. There appears to be some differences in the values of $\langle S_z \rangle$ which we calculate and the values used to calculate magnetic moments in work of Lamm.[8] These differences occur only in some of the positive-parity ($N = 6$) single-particle states.

One thing to learn from Fig. 1 is the limitation of the effects of equipotential surface deformation

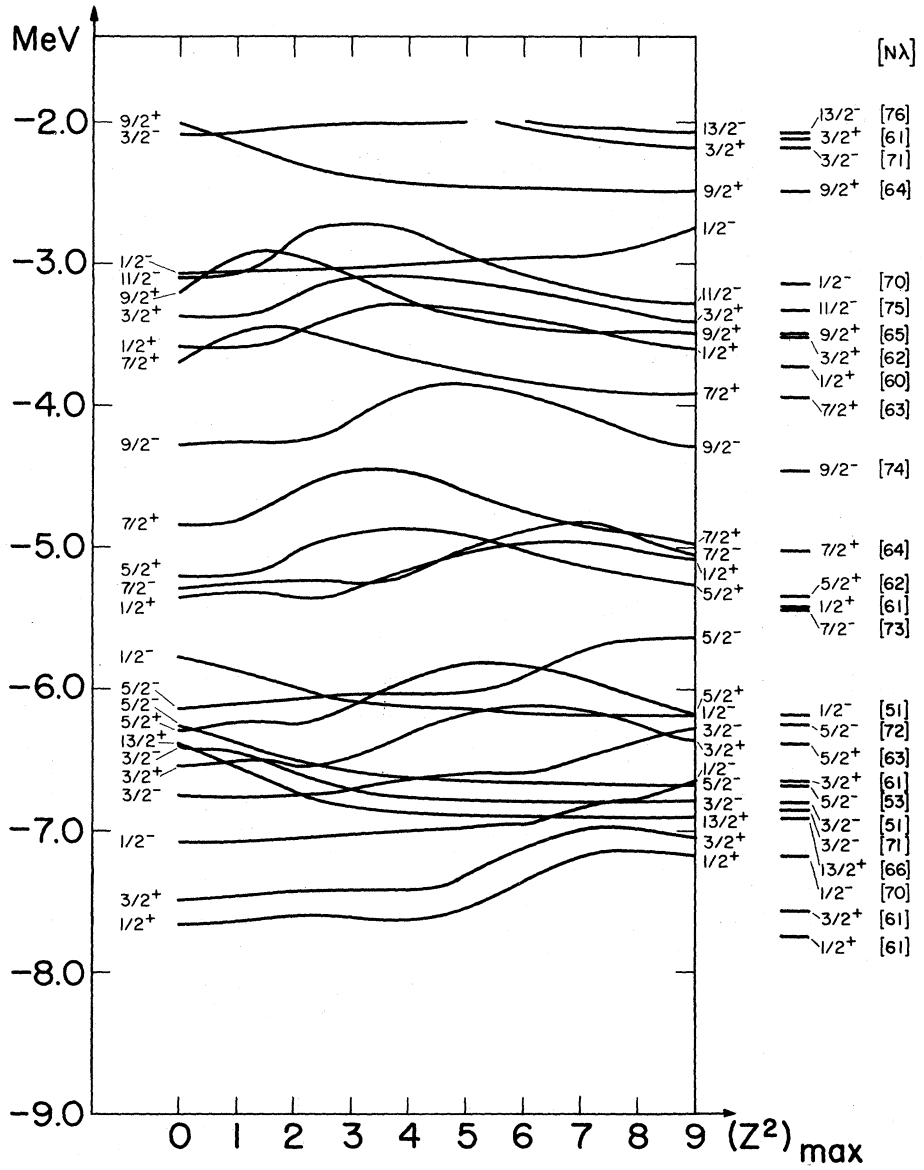

FIG. 2. Shifts of single-particle energies for positive $G(z^2)$. The results in this figure are obtained by reflecting the single-particle shifts of Fig. 1, as explained in the text.

on single-particle energy spacings. If two states move in tandem as a function of $z^2{}_{max}$, it seems rather unlikely that we could account for an experimental crossing of these states with any axially symmetric equipotential shape variation. To put this observation in somewhat more concrete terms, we consider some of the low-energy neutron states observed in ^{245}Cm and ^{247}Cm. From the (d,p) and (d,t) reaction studies, we infer that in ^{245}Cm, the ground state has a spin of $\frac{7}{2}^+$; the first hole state, a spin of $\frac{5}{2}^+$; and the first particle state, a spin of $\frac{9}{2}^-$. In ^{247}Cm, we infer a ground-state spin of $\frac{9}{2}^-$, a first hole state of spin $\frac{5}{2}^+$, and a second hole state of spin $\frac{7}{2}^+$. This is illustrated in Fig. 3.

When we examine the appropriate levels ($\frac{5}{2}^+[62]$ and $\frac{7}{2}^+[64]$) in Fig. 1, we see that they tend to stay about the same distance apart from each other for all values of $z^2{}_{max}$. This observation suggests that distorting equipotential surfaces in an axially symmetric way is not going to help us understand this experimentally observed crossing.

We have tried to find an equipotential shape which gives energies in good agreement with the experimentally observed energy level spacings in ^{235}U. We note first that one obtains a fairly good fit to the data by assuming that ^{235}U is ellipsoidal; this is illustrated in Fig. 4. In the first column of Fig. 4, we have plotted a set of single-particle en-

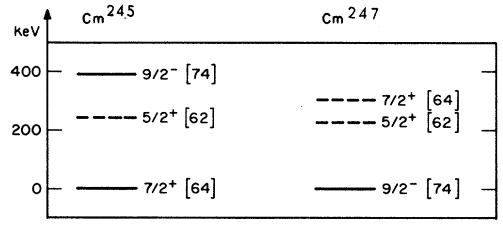

FIG. 3. Low-lying band heads in ^{245}Cm and ^{247}Cm. The information is obtained from the Table of Isotopes (John Wiley & Sons, Inc., New York, 1967), and (d,p) and (d,t) experimental data (see Ref. 9) currently being analyzed. Hole states are indicated by dashed lines.

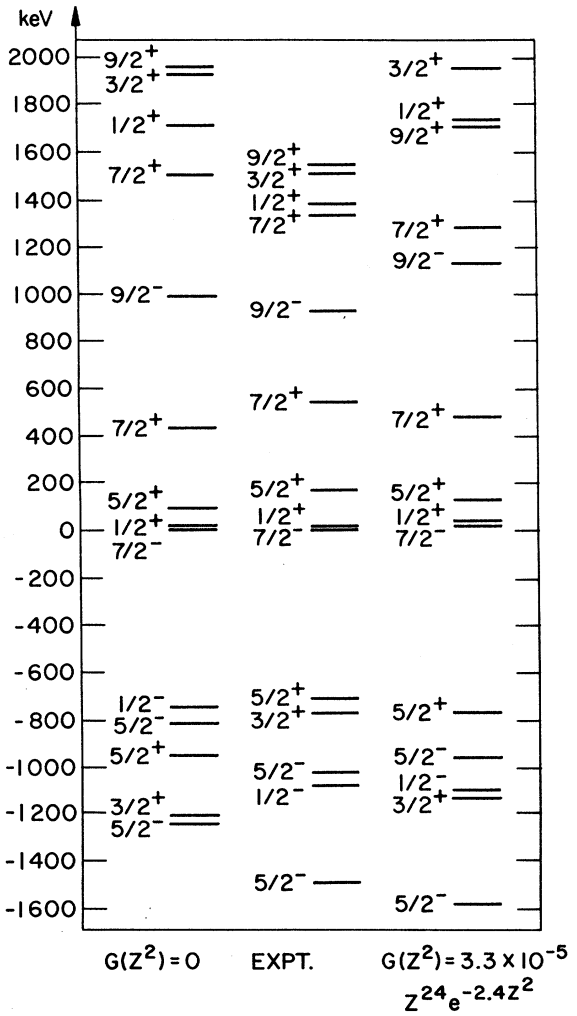

FIG. 4. Comparison of calculated and observed single-particle states in ^{235}U. The calculated values of column 1 are obtained with the parameters used in Fig. 1, with $G(z^2)=0$. The experimental (see Ref. 9) values of column 2 have been corrected for pairing effects. The calculated values of column 3 are obtained with the parameters of Fig. 1, with the changes $K'=0.134$ MeV and $G(z^2)=3.3\times10^{-5}z^{24}e^{-2.4z^2}$.

TABLE I. Expansion of $G(\cos^2\theta)$ of Eq. (13′) in terms of Legendre polynomials.

l	$\int_0^\pi G(\cos^2\theta)P_l(\cos\theta)\sin\theta\,d\theta$
0	+0.0191
2	+0.0191
4	−0.0079
6	−0.0126
8	+0.0014
10	+0.0053

ergies computed under the assumption that $G(z^2)=0$; and in the second column, we give the experimentally[9] determined single-particle energies (energy shifts due to pairing forces[10] have been removed from the experimental data). The main discrepancy between calculation and experiment occurs for the hole states of ^{235}U; also some of the particle states occur at too high an energy in the calculation. From Fig. 2 we can see that the hole-state spectrum would be improved by choosing $G(z^2)$ such that $z^2{}_{\max}\approx 5$. In the third column of Fig. 4, we display a single-particle spectrum computed under the assumption that

$$G(z^2)=3.3\times10^{-5}(z^{24}e^{-2.4z^2}), \tag{13}$$

and this leads to a marked improvement in the agreement with the experimental spectrum. The major remaining discrepancies are in the energies of the $\frac{3}{2}^+[61]$ hole state, and the $\frac{3}{2}^+[62]$, and $\frac{1}{2}^+[60]$ particle states. Undoubtedly, there are other choices of peak height and width that give roughly the same single-particle spectrum; the essential features appear to be that $z^2{}_{\max}\approx 5$ and that the sign of $G(z^2)$ be positve. There is no great resemblance between this form of $G(z^2)$ and a deformation of the form $P_4^0(\cos\theta)$; perhaps we might say that it corresponds roughly to the peak at 0° for levels in the $N=5$ and $N=6$ oscillator shells.

It is, of course, possible to expand the function $G(z^2)$ in Legendre polynomials on any surface of constant R^2. For $R^2=8$, we have

$$G(\cos^2\theta)=2.27\times10^6\cos^{24}\theta\,e^{-19.2\cos^2\theta}. \tag{13′}$$

In the table, we list the first six nonzero coefficients in the Legendre expansion of this function.

In Fig. 5, we show the equipotential shape implied by the $G(z^2)$ of Eq. (13) as well as the equipotential shape of an ellipse of the same deformation radius and a circle of the same radius. In Fig. 6, we give a somewhat more complete calculated single-particle spectrum for ^{235}U which includes some states not yet seen in ^{235}U. The calculations are done with the $G(z^2)$ given in Eq. (13) and pairing interactions[10] are also included in the calculated

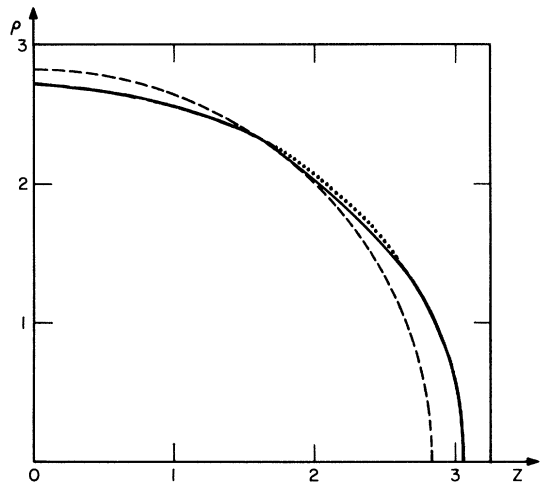

FIG. 5. Equipotential shapes. The solid line represents the equipotential shape used for ^{235}U setting $R_0^2 = 8$. With dashed lines, we show the deviation from the elliptical shape obtained by setting $G(z^2) = 0$. We also show the circle obtained by setting $\epsilon = 0$.

spectrum; so this calculated spectrum can be compared directly with experimentally observed single-particle energies. We hope that it will be of value in future experimental studies.

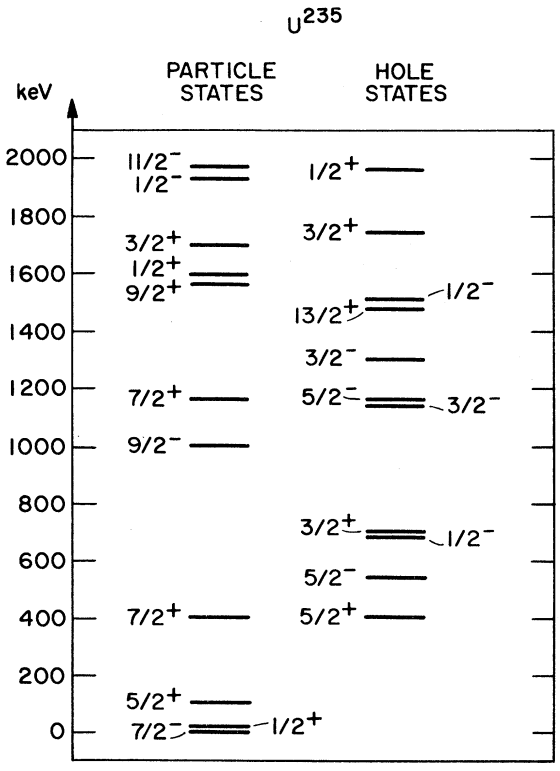

FIG. 6. Predicted energies of single-particle states in ^{235}U. Pairing effects are included in this calculation of the excitation energies of single-particle band heads.

In the hope of saving others some unfruitful labor, we mention an approach for improving the agreement between calculated and observed single-particle energies in ^{235}U that we believe to be incorrect. The main difficulty in the calculated single-particle spectrum is that the hole states $\frac{1}{2}^-[51]$, $\frac{5}{2}^-[53]$, and $\frac{5}{2}^-[72]$ are too close to ground. The $N = 5$ shell levels can be moved farther away from the ground state by making some changes in the radial form of the Woods-Saxon potential and keeping $G(z^2) = 0$. By making the potential well somewhat deeper at the origin, i.e., making the replacement

$$\frac{1}{1+e^{\alpha[(r/R_0)-1]}} \rightarrow \frac{1}{1+e^{\alpha[(r/R_0)-1]}} + K_1 e^{-K_2(r/R_0)^2} \tag{14}$$

and suitably choosing parameters, it is possible to obtain improvements in the calculated single-particle energies relative to experiment for ^{235}U. The $N = 5$ hole states are moved further away from the Fermi surface. However, one also gets single-particle wave functions that appear to be quite unrealistic; i.e., bear little resemblance to the expected asymptotic labeling.

IV. SUMMARY AND CONCLUSIONS

The possibility of explaining observed spectra is considerably increased by allowing general axially symmetric deformations of the equipotential surfaces. Figures 1 and 2 of this paper indicate many of the changes in level ordering and spacing that can be made in this way. They also indicate the limitations of this class of deformation in shifting ordering of levels. The approach appears to be useful in a study of ^{235}U, but quite powerless to explain a level inversion between ^{245}Cm and ^{247}Cm.

In order to see the ultimate limitations of single-particle models, calculations must be made in which the restriction to axially symmetric shapes is dropped. This would seem to involve a herculean calculational effort. When and if such calculations are made, we should be in a position to answer the fundamental question: how well can simple models consisting of single-particle interactions and residual pairing forces account for low-energy excitations observed in real nuclei?

V. ACKNOWLEDGMENTS

I thank I. Ahmad, T. Braid, J. Erskine, and A. Friedman for keeping me constantly aware of experimental data on single-particle states; B. Garbow for a great deal of help in the programming associated with this problem; and D. Kurath and R. Lawson for constructive comments and criticisms on this work. Finally, I thank S. G. Nilsson for generous help in the early phases of this study.

APPENDIX A

We present here some relations needed for the computation of matrix elements, many of which can be found[5] in the literature.

For computing matrix elements of p_z^2 and p_ρ^2, we note

$$\langle n_z | p_z^2 | n_z \rangle = \langle n_z | z^2 | n_z \rangle ,$$
$$\langle n_z | p_z^2 | n_z' \rangle = -\langle n_z | z^2 | n_z' \rangle , \tag{A1}$$

with similar relations holding between ρ^2 and p_ρ^2. We have

$$z^2 | n_z \rangle = (n_z + \tfrac{1}{2}) | n_z \rangle + \tfrac{1}{2}[(n_z+1)(n_z+2)]^{1/2} | n_z + 2 \rangle + \tfrac{1}{2}[n_z(n_z-1)]^{1/2} | n_z - 2 \rangle , \tag{A2}$$

and

$$\rho^2 | n_\perp, \lambda \rangle = (n_\perp + 1) | n_\perp, \lambda \rangle + \tfrac{1}{2}[(n_\perp + \lambda + 2)(n_\perp - \lambda + 2)]^{1/2} | n_\perp + 2, \lambda \rangle + \tfrac{1}{2}[(n_\perp - \lambda)(n_\perp + \lambda)]^{1/2} | n_\perp - 2, \lambda \rangle . \tag{A3}$$

We evaluate matrix elements of the form

$$\langle n_\perp, \lambda | \rho^{2k} e^{-m\rho^2} | n_\perp', \lambda' \rangle \quad \text{and} \quad \langle n_z | z^{2k} e^{-mz^2} | n_z' \rangle$$

by direct integration. Explicit forms for the basis states are

$$| n_z \rangle = \frac{\pi^{-1/4} e^{-z^2/2}}{[2^{n_z}(n_z!)]^{1/2}} \sum_J \frac{(-1)^J (n_z!)}{(J!)(n_z - 2J)!} z^{(n_z - 2J)} , \tag{A4}$$

and

$$| n_\perp, \lambda \rangle = \frac{\rho^\lambda e^{-\rho^2/2} e^{i\lambda\varphi}}{(2\pi)^{1/2}} \left[\left(\frac{n_\perp - \lambda}{2} \right)! \left(\frac{n_\perp + \lambda}{2} \right)! \right]^{1/2} \sum_J \frac{(-1)^J \rho^{2[(n_\perp - \lambda)/2 - J]}}{J! \left[\left(\frac{n_\perp - \lambda}{2} \right) - J \right]! \left[\left(\frac{n_\perp + \lambda}{2} \right) - J \right]!} , \tag{A5}$$

where J is constrained to those integer values in Eqs. (A4) and (A5) such that the factorials are nonnegative integers.

Finally, we need matrix elements of $\vec{l} \cdot \vec{s}$. The diagonal elements are

$$\langle n_\perp, \lambda, n_z, \pm\tfrac{1}{2} | l_z s_z | n_\perp, \lambda, n_z, \pm\tfrac{1}{2} \rangle = \pm\tfrac{1}{2}\lambda , \tag{A6}$$

and the nonvanishing off-diagonal matrix elements needed in the calculation are

$$\langle n_\perp - 1, \lambda + 1, n_z + 1, -\tfrac{1}{2} | \vec{l} \cdot \vec{s} | n_\perp, \lambda, n_z, +\tfrac{1}{2} \rangle = \tfrac{1}{4}(e^{\epsilon/2} + e^{-\epsilon/2})[(n_z+1)(n_\perp - \lambda)]^{1/2} , \tag{A7}$$

$$\langle n_\perp + 1, \lambda + 1, n_z - 1, -\tfrac{1}{2} | \vec{l} \cdot \vec{s} | n_\perp, \lambda, n_z, \tfrac{1}{2} \rangle = -\tfrac{1}{4}(e^{\epsilon/2} + e^{-\epsilon/2})[n_z(n_\perp + \lambda + 2)]^{1/2} , \tag{A8}$$

$$\langle n_\perp + 1, \lambda + 1, n_z + 1, -\tfrac{1}{2} | \vec{l} \cdot \vec{s} | n_\perp, \lambda, n_z, \tfrac{1}{2} \rangle = -\tfrac{1}{4}(e^{\epsilon/2} - e^{-\epsilon/2})[(n_z+1)(n_\perp + \lambda + 2)]^{1/2} , \tag{A9}$$

and

$$\langle n_\perp - 1, \lambda + 1, n_z - 1, -\tfrac{1}{2} | \vec{l} \cdot \vec{s} | n_\perp, \lambda, n_z, \tfrac{1}{2} \rangle = \tfrac{1}{4}(e^{\epsilon/2} - e^{-\epsilon/2})[n_z(n_\perp - \lambda)]^{1/2} , \tag{A10}$$

together with the relation

$$\langle a | \vec{l} \cdot \vec{s} | b \rangle = \langle b | \vec{l} \cdot \vec{s} | a \rangle . \tag{A11}$$

We note that it makes very little difference if the $N, N+2$ matrix elements of $\vec{l} \cdot \vec{s}$ are set equal to zero, and K' is adjusted slightly.

---

*Work performed under the auspices of the U. S. Atomic Energy Commission.

[1]S. G. Nilsson, Kgl. Danske Videnskab. Selskab, Mat.-Fys. Medd. 29, No. 16 (1955).

[2]E. Rost, Phys. Rev. 154, 994 (1967).

[3]S. G. Nilsson, in Nuclear Structure and Nuclear Reaction, Proceedings of the International School of Physics "Enrico Fermi," Course XL, 1967, edited by M. Jean (Academic Press Inc., New York, 1969).

[4]F. A. Gareev, S. P. Ivanova, and B. N. Kalinkin, Joint Institute for Nuclear Research (Dubna) Report No. JINR P4-3451, 1967 (to be published); F. A. Gareev, S. P. Ivanova, B. N. Kalinkin, S. K. Slepnev, and M. G. Ginzburg, Joint Institute for Nuclear Research (Dubna) Report No. JINR P4-3607, 1967 (to be published).

[5]A. J. Rassey, Phys. Rev. 109, 949 (1958).

[6]R. R. Chasman and S. Wahlborn, Nucl. Phys. A90, 401 (1967).

[7]A. A. Ross, H. Mark, and R. D. Lawson, Phys. Rev. 102, 1613 (1956).

[8]I. L. Lamm, Nucl. Phys. A125, 504 (1969).

[9]T. H. Braid, R. R. Chasman, J. R. Erskine, and A. M. Friedman, Phys. Rev. C 1, 275 (1970).

[10]R. R. Chasman, Phys. Rev. 134, B279 (1964).